Available online at www.sciencedirect.com
SCIENCE DIRECT®
Journal of Power Sources 149 (2005) 22–32
JOURNAL OF POWER SOURCES
www.elsevier.com/locate/jpowsour

Influence of the anodic recirculation transient behaviour on the SOFC hybrid system performance

Mario L. Ferrari *, Alberto Traverso, Loredana Magistri, Aristide F. Massardo

Thermochemical Power Group (TPG), Dipartimento di Macchine, Sistemi Energetici e Trasporti, Università di Genova, Italy

Received 7 October 2004; received in revised form 27 January 2005; accepted 31 January 2005
Available online 13 April 2005

Abstract

This paper addresses the off-design and transient response of a high efficiency hybrid system based on the coupling of a recuperated micro-gas turbine (mGT) with a tubular solid oxide fuel cell (SOFC) reactor.

The work focuses on the anodic side where an ejector exploits the pressure energy of the fuel to recirculate part of the exhaust gas, in order to maintain a proper value for the steam-to-carbon ratio (STCR) and to support the reforming reactions. Two different stand-alone time-dependent ejector models are presented and validated against experimental data. Then, the most suitable model for cycle simulations, in term of calculation time, has been employed for the transient analysis of the entire hybrid system.

The SOFC hybrid system transient behaviour is presented and discussed at several operating conditions from an electrochemical, fluid dynamic and thermal point of view.

Keywords: Ejector; Anodic recirculation; SOFC; Hybrid system

1. Introduction

Hybrid fuel cell systems are considered to be a good candidate for the future power generation because of their high efficiency and ultra-low emissions. Especially solid oxide fuel cell (SOFC) hybrid systems, because of their very high efficiency due to a better use of the free Gibbs energy and high operative temperatures, seem to be the right answer to overcome the Carnot efficiency, that is the main limitation of traditional power plants. Moreover, the high temperature exhaust gas can be well exploited for distributed cogeneration.

Even if the SOFC–HS steady-state analysis has already been carried out in previous works [1,2], a transient investigation still remains necessary. In fact, while the SOFC hybrid system study at on-design and off-design conditions is necessary for assessing the cycle performance and understanding the safe operative limits of plants, the transient analysis is mandatory for implementing the control system and studying the critical aspects with time. In fact, it is extremely useful for avoiding malfunctions or damage to the key-components of the plant, especially during the start-up/shut-down or during rapid load variations. In a SOFC hybrid system the main risk situations are, for instance, (I) an excessive temperature in the fuel cell, (II) too high a pressure difference between the cathodic and the anodic sides, (III) too low an STCR value in the reformer, (IV) too high a microturbine rotational speed, (V) an operating condition too close to the compressor surge line (surge margin) or (VI) excessive thermal stress in the heat exchanger and the cell. All these constraints need to be coped with during both load regulation and start-up/shut-down procedures.

The results presented in this work refer to the classic scheme of an SOFC–HS with a recuperated mGT [3], previously investigated at design and off-design conditions [1].

* Corresponding author. Tel.: +39 010 3532463; fax: +39 010 353 2566.
E-mail address: mario.ferrari@unige.it (M.L. Ferrari).

0378-7753/$ – see front matter © 2005 Elsevier B.V. All rights reserved.
doi:10.1016/j.jpowsour.2005.01.059

Nomenclature

a	sound speed ($m\,s^{-1}$)
A	cross sectional area (m^2)
c, u	velocity ($m\,s^{-1}$)
C_{dis}	discharge coefficient
c_p	constant pressure specific heat ($J\,(kg\,K)^{-1}$)
c_v	constant volume specific heat ($J\,(kg\,K)^{-1}$)
D	diameter (m)
f	friction factor
h	convection coefficient ($W\,(m^2\,K)^{-1}$)
HS	hybrid system
i	current density ($mA\,(cm^2)^{-1}$)
k	c_p/c_v
K_p	surge margin
L	length (m)
LHV	low heating value ($J\,kg^{-1}$)
$\dot{m}$	mass flow ($kg\,s^{-1}$)
mGT	micro gas turbine
Ma	Mach number
Mass	mass (kg)
N	rotational speed (rpm)
p	pressure (Pa)
P	power (W)
q	heat flux (W)
Re	Reynolds number
S	heat transfer surface (m^2)
SOFC	solid oxide fuel cell
STCR	steam-to-carbon ratio
t	time (s)
Δt	time increase (s)
T	temperature (K)
TOT	turbine outlet temperature (K)
U_f	fuel utilization coefficient
V	volume (m^3)
x	mass flow direction (m)
Δx	distance between calculation sections (m)
XMA	mass fractions

Greek symbols

α	diffuser angle (rad)
β	pressure ratio
ε	recuperator effectiveness
η	efficiency
ρ	density ($kg\,(m^3)^{-1}$)

Subscripts

0	on-design
1	primary duct outlet
2	secondary duct outlet
3	diffuser inlet
4	diffuser outlet
a, b	heat exchange surfaces
amb	ambient
av	average
diff	diffuser
ext	external
FC	fuel cell
f	friction
fuel	fuel
HS	hybrid system
i,i+1	calculation section number
in	inlet
int	internal
iso	isoentropic
metal	metal
mGT	micro gas turbine
mix	mixing chamber
out	outlet
prim	primary
sec	secondary
s.l.	surge line
t	total

Superscripts

$'$	on-design

2. The plant

The hybrid system studied in this work is a plant of about 300 kW net electrical power, employing a microturbine integrated with a tubular pressurized SOFC (Fig. 1). The cell cathode receives the air from a pre-heater downstream the compressor. The anodic side uses the gas mixture coming from the reformer, which partially converts the fuel (methane) into hydrogen. The SOFC exhaust gases are fed into a post-combustor to increase turbine inlet enthalpy. Part of the anodic flow is mixed with the fuel and recirculated at the anode inlet (Fig. 2). This is necessary to generate the right temperature for the reforming reactions and to avoid carbon deposition inside the reformer and the stack. In fact, if the steam-to-carbon ratio (STCR) value inside this component is reduced, carbon deposits irreparably damage both the reformer and the cell stack. This recirculation system is mainly composed by a single-stage ejector [4] (Fig. 3) where the fuel is introduced through a primary nozzle. The primary flow must have high momentum to ensure the proper recirculation ratio, and to create the pressure increase to compensate the pressure drop inside the fuel cell.

The anodic side is mainly dependent on the ejector performance, so a complete analysis of this component is essential. Therefore, in this paper, two anodic ejector models are described and validated. The first detailed model, based on the 1D-CFD equations, is useful to evaluate the local phenomena, such as shock waves, but requires a very long calculation time, mainly when used at the system level. For this reason a simplified model has been developed and used for the whole plant simulations.

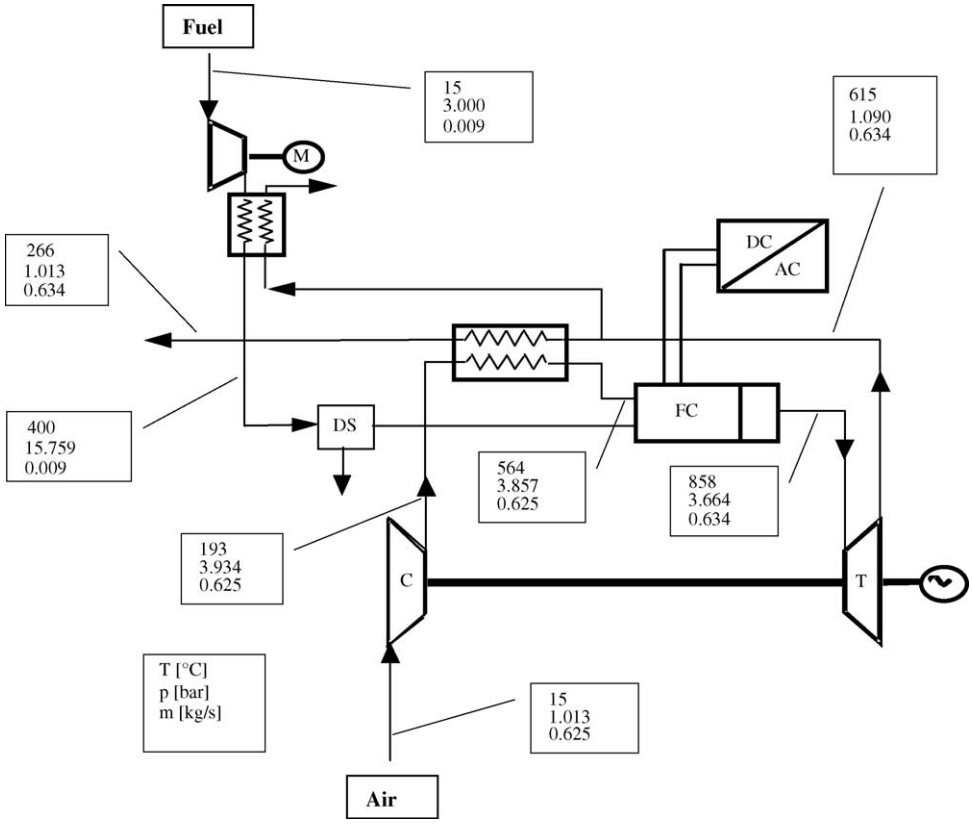

Fig. 1. Hybrid system plant-layout. $P_{HS} = 289\,kW$, $P_{FC} = 239\,kW$, $Pm_{GT} = 50\,kW$, $\eta_{el} = 0.64$.

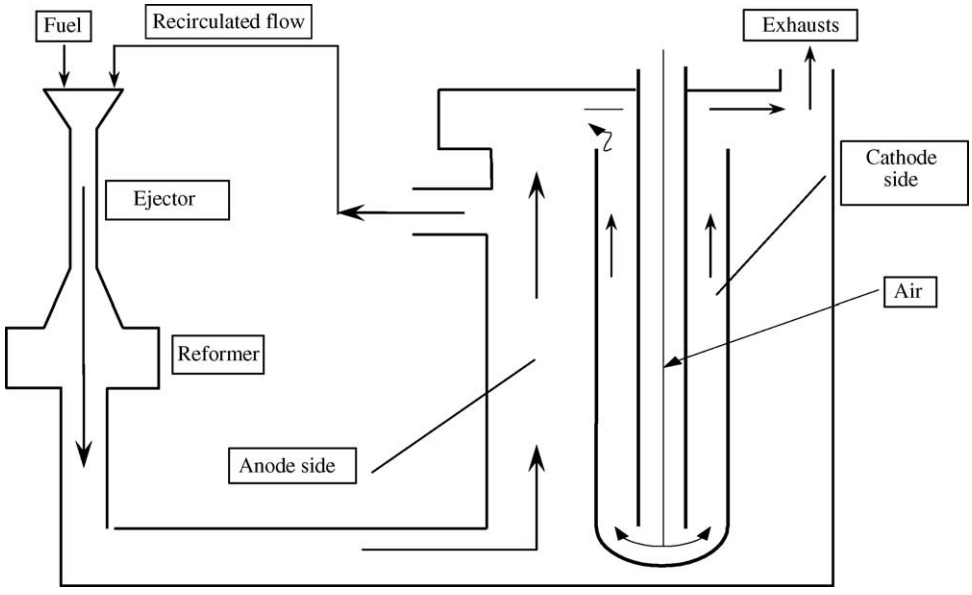

Fig. 2. Anodic circuit of a tubular SOFC.

3. Ejector models

The "dynamic" ejector model is based on the one-dimensional Euler fluid dynamic equations with source terms, integrated using an explicit scheme [5]. The method, even if less accurate than more modern integration schemes, is useful and effective for plant simulations, because it shows the main fluid dynamic phenomena with a good flexibility for the introduction of source terms for viscous pressure losses, heat exchanges, and so forth.

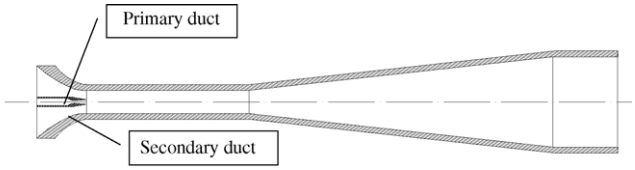

Fig. 3. Ejector scheme.

The "dynamic" ejector model is based on the hypothesis of adiabatic flow and semi-ideal gas, that is $p = \rho RT$ and variable specific heats, resulting from temperature and composition.

To analyse the anodic transient recirculation behaviour, it is necessary to evaluate the composition variation over time. So, the "dynamic" model applies the following equations to the duct:

$$\dot{m}_i = \dot{m}\,\mathrm{XMA}_i \quad (i \text{ is the chemical element number}) \tag{1}$$

$$\mathrm{Mass}_i = \rho_{\mathrm{av}}\, V\, \mathrm{XMA}_i \tag{2}$$

$$\frac{\partial \mathrm{Mass}_i}{\partial t} = \dot{m}_{i\_\mathrm{in}} - \dot{m}_{i\_\mathrm{out}} \tag{3}$$

The model is general because it employs gas mixtures of 28 gases [3].

The 1D conservative form equations are:

$$\frac{\partial \bar{U}}{\partial t} + \frac{\partial \bar{F}}{\partial x} = \bar{Q} \tag{4}$$

where:

$$\bar{U} = \begin{bmatrix} \rho A \\ \rho A c \\ \rho A \left(c_v T + \dfrac{c^2}{2} \right) \end{bmatrix} \quad \bar{F} = \begin{bmatrix} \rho A c \\ \rho A c^2 + pA \\ \rho A c \left(c_p T + \dfrac{c^2}{2} \right) \end{bmatrix}$$

$$\bar{Q} = \begin{bmatrix} 0 \\ p \dfrac{\partial A}{\partial x} \\ 0 \end{bmatrix} \tag{5}$$

The ejector is divided into N calculation cells where the equations are numerically integrated, leaving out the extreme sections. The explicit scheme [6] is based on two steps: "predictor" and "corrector".

The boundary sections are solved with the method of characteristics [7,8]:

$$\mathrm{d}p - \rho a\, \mathrm{d}u = 0 \quad \text{for the characteristic} \quad \frac{\mathrm{d}x}{\mathrm{d}t} = u - a \tag{6}$$

$$\mathrm{d}p + \rho a\, \mathrm{d}u = 0 \quad \text{for the characteristic} \quad \frac{\mathrm{d}x}{\mathrm{d}t} = u + a \tag{7}$$

The Eqs. (6) and (7) must be applied where $\partial A/\partial x = 0$ and there are no source terms.

The viscous pressure losses are introduced with the following source term:

$$(\mathrm{Source\_pdc})_i = \frac{A_{i+1} + A_i}{2} \frac{\Delta p_{f_i}}{\Delta x} \tag{8}$$

where

$$\Delta p_{f_i} = \rho_i \frac{c_i^2}{2} f_i \frac{\Delta x}{D_i} \tag{9}$$

$$f_i = f' \left(\frac{Re'}{Re_i} \right)^{\alpha} \tag{10}$$

To simulate the different fluid dynamic phenomena of the ejector ducts (convergent, mixing chamber, diffuser), the code allows for the introduction of three different values of Re' and f' which are the references at on-design conditions [9].

So, the vector $\bar{Q}$ becomes:

$$\bar{Q} = \begin{bmatrix} 0 \\ p_{\mathrm{av}} \dfrac{A_{i+1} - A_i}{\Delta x} - (\mathrm{Source\_pdc})_i \\ 0 \end{bmatrix},$$

$$p_{\mathrm{av}} = \frac{p_i + p_{i+1}}{2} \tag{11}$$

The ejector mixing-chamber is also modelled with the source term technique. In fact the injection of the primary nozzle flow into the secondary flow is simulated introducing further source terms into the vector $\bar{Q}$. So the code calculates, with the isentropic and (if necessary) normal wave equations, the mass flow, the momentum and the total enthalpy at the primary nozzle outlet [9]. The whole primary mass flow is introduced into the first mixing camera cell, while the momentum and the total enthalpy are injected into the entire mixing chamber with an apt triangular distribution (Fig. 4).

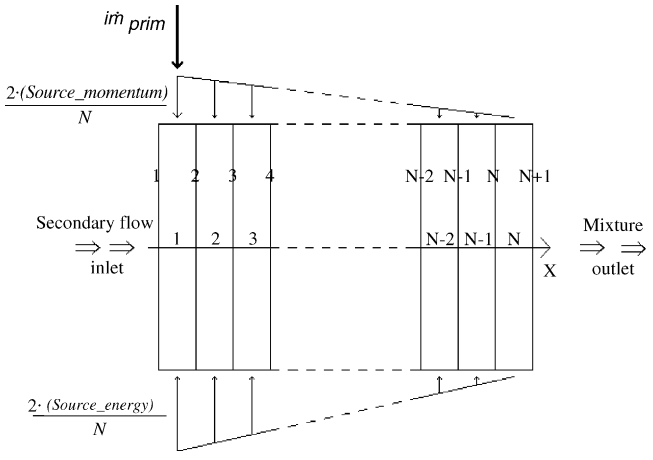

Fig. 4. Mixing chamber source terms.

In detail:

$$\text{(Source\_momentum)} = C_{\text{dis}}\dot{m}_{\text{prim}}c_{\text{out\_prim}} + A_{\text{out\_prim}}(p_{\text{iso}} - p_{\text{out\_sec}}) \quad (12)$$

$$\text{(Source\_energy)} = \dot{m}_{\text{prim}}\text{enthalpy}_{\text{t\_prim}} \quad (13)$$

Since the reduction of the calculation time is a necessary requirement when plant simulations are carried out, a "lumped volume" ejector model has been developed as well. Such a model accepts an integration time step about 100 times higher than the "dynamic" model one described before, with a large reduction in calculation time. In fact the "lumped volume" model does not require any calculation grid, but the equations are integrated into the whole ejector volume. So, the integration time step does not have to satisfy the well-known "dynamic" model stability rule [10].

The "lumped volume" model is a simplified scheme for a constant mixing camera ejector, also based on the hypothesis of semi-ideal gas. The treatment of the composition variation over time is the same as for the "dynamic" model. It is important to highlight the introduction of heat exchange in the "lumped volume" model. In fact, even if the ejector could be considered adiabatic at steady-state conditions, experimental tests [11] show that transient heat exchange with the material may not be negligible.

The "lumped volume" model is formed by an off-design model and by a constant area pipe for the fluid dynamic delay.

The actuator disk is based on the mass, momentum and energy steady-state equations:

$$\dot{m}_3 = \dot{m}_1 + \dot{m}_2 \quad (14)$$

$$p_3A_3(1 + k_3Ma_3^2) = p_1A_1(1 + k_1C_{\text{dis}}Ma_1^2) + p_2A_2(1 + k_2Ma_2^2) \quad (15)$$

$$\dot{m}_3\left(h_3 + \frac{c_3^2}{2}\right) = \dot{m}_1\left(h_1 + \frac{c_1^2}{2}\right) + \dot{m}_2\left(h_2 + \frac{c_2^2}{2}\right) \quad (16)$$

The viscous pressure losses are only introduced into the mixing chamber (Eq. (17)) and the diffuser (Eq. (18)) because they are negligible in the secondary convergent duct.

$$\Delta p_f = \rho_{\text{av\_mix}}\frac{c_{\text{av\_mix}}^2}{2}f\frac{L_{\text{mix}}}{D_{\text{mix}}} \quad (17)$$

$$\Delta p_f = \frac{C_f}{4\alpha}\left(1 - \frac{1}{(A_4/A_3)^2}\right) + \alpha\left(1 - \frac{1}{(A_4/A_3)}\right)^2\rho_{\text{av\_diff}}\frac{c_{\text{av\_diff}}^2}{2} \quad (18)$$

where C_f is a friction coefficient and the average quantities are calculated with simple arithmetical averages between the inlet and the outlet of the components.

Fig. 5. Ejector used for validation (length: 0.686 m) [12].

The time-dependent behaviour is predicted based on the following equations:

$$\frac{d\dot{m}_4}{dt} = \frac{A}{L}[C - (p_{\text{out}} - p_{\text{t\_in}})] \quad (19)$$

$$\frac{d(c_{v_4}\text{Mass}T_{t_4})}{dt} = \Delta(\dot{m}c_pT_t) + q_{\text{metal}} \quad (20)$$

$$\frac{dT_{\text{metal}}}{dt} = \frac{q}{\text{Mass}_{\text{metal}}c_{v_{\text{metal}}}} \quad (21)$$

where C is the pressure rise across the ejector and:

$$q = q_{\text{amb}} + q_{\text{metal}} = S_{\text{int}}h(T_{\text{av\_eject}} - T_{\text{metal}}) + S_{\text{ext}}h_{\text{amb}}(T_{\text{amb}} - T_{\text{metal}}) \quad (22)$$

The ejector material average temperature in Eq. (21) is necessary for the introduction of the heat exchange source term into (22).

The "dynamic" ejector model has been validated at steady-state conditions with a comparison between experimental data [12] and the model results. The test ejector (Fig. 5) is rectangular with a convergent sonic primary nozzle. Introducing dry air into both ducts, and with reasonable values for viscous pressure losses, the model calculates the experimental data [12] with great accuracy, as shown in Fig. 6. These results represent a good validation of the original source term distribution proposed in this work (Fig. 4). This model has been verified for unsteady conditions studying shock wave propagation, with a "Shock tube" approach [13].

The "lumped volume" model has been compared to the previous "dynamic" model. For example, considering a primary total pressure step (10% reduction), an ejector designed for SOFC anodic recirculation shows that both models calculate the same steady-state off-design performance. Referring

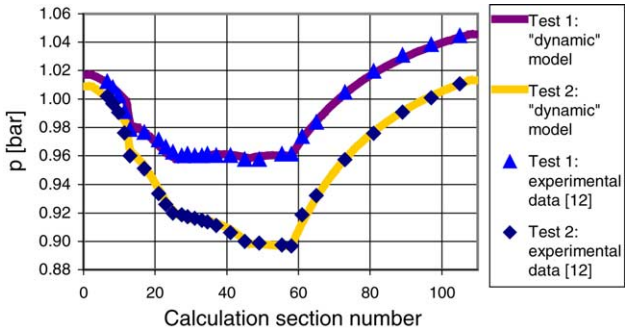

Fig. 6. Comparison between theoretical and experimental static pressure distribution for the ejector tested in [12].

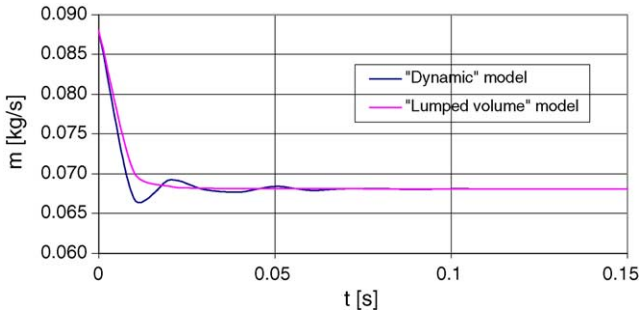

Fig. 7. Diffuser outlet mass flow: comparison of "dynamic" and "lumped volume" model.

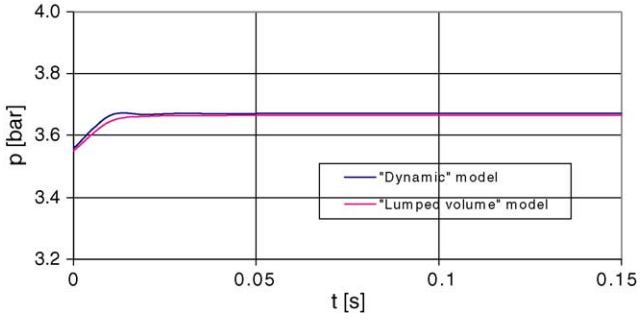

Fig. 8. Diffuser inlet static pressure: comparison of "dynamic" and "lumped volume" model.

to the transient behaviour, the "lumped volume" is capable of getting the same time response scale (Figs. 7 and 8) and the average behaviour over time.

A complete experimental validation including transient results with an apt test rig of the anodic ejector (Fig. 9) is at the moment in progress at TPG laboratory, under the European FP-V contract PIP–SOFC.

4. Hybrid system transient model

The hybrid system transient model was implemented using the TRANSEO tool [14] developed at TPG within the MATLAB-Simulink environment [15], to exploit the MATLAB mathematical functions and to create a visual, user-friendly, modular code. All the TRANSEO models take into account the chemical composition variation with time with the algorithm presented for the ejector "dynamic" model. In fact, in hybrid systems the chemical composition of streams can show significant changes, which affect the matching of fuel cell and turbomachinery at both steady-state and transient conditions. It is worth noting that all the component models take into account the heat exchange with the walls, which are not negligible over long-time scales.

The quasi 2D recuperator model, which has been described in [14,16], takes into account the following aspects: (I) flow fluid dynamic inertia; (II) metal matrix and vessel thermal inertia; (III) variation in convective heat transfer coefficient; (IV) variation in viscous pressure loss; (V) variation in internal matrix fin efficiency. The SOFC simplified model, which has been described in [2], is set on the tubular geometry presented in [17]. The analysis of the system has been performed in three steps: (1) design point definition; (2) off-design analysis; (3) transient behaviour.

4.1. Design point definition

The hybrid system design point was chosen to optimise the plant efficiency without generating excessive thermal and mechanical stresses. In fact, even if the SOFC performance increases with cell temperature, there is a limitation (950–1000 °C depending on the materials) to avoid damage to the ceramics and to not reduce the life of the system. So, fuel and air mass flows were chosen to satisfy this operational

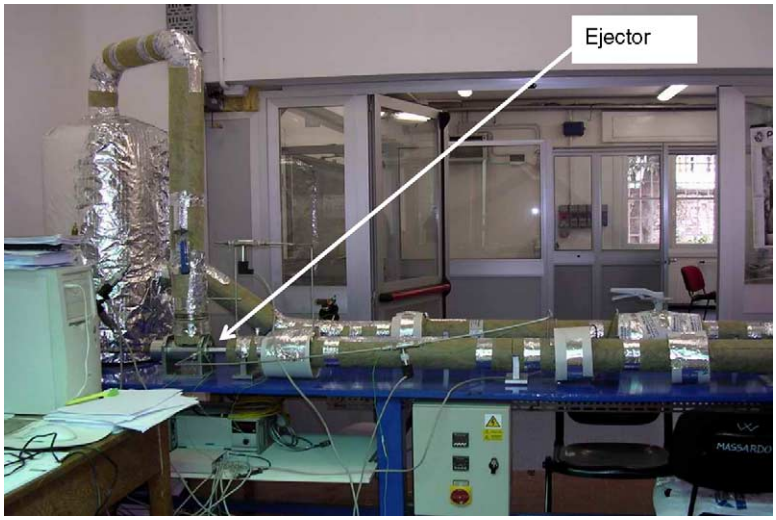

Fig. 9. TPG-UNIGE Ejector test rig.

Table 1
On-design values

Ejector	
Fuel mass flow (primary flow) (kg s^{-1})	0.009
Fuel composition (CH_4) (%)	100
Recirculation mass flow ratio	7.2
Tubular SOFC	
Reaction pressure (bar)	3.74
Air inlet temperature (K)	873
Cathode mass flow (kg s^{-1})	0.625
Fuel utilization coefficient	0.85
Electrical power (kW)	238.8
Efficiency	0.53
Current density (mA (cm^2)$^{-1}$)	426.9
Compressor	
Power (kW)	112.7
Isentropic efficiency	0.76
Rotational speed (rpm)	68000
Pressure ratio	3.88
Mass flow (kg s^{-1})	0.625
Expander (turbine)	
Power (kW)	182.2
Isentropic efficiency	0.84
Rotational speed (rpm)	68000
Expansion ratio	3.36
Mass flow (kg s^{-1})	0.634
Recuperator	
Effectiveness	0.88
Fuel compressor	
Power (kW)	9.4
Isentropic efficiency	0.6
	Generator
Mechanical efficiency	0.95
Electrical efficiency	0.88
System (taking into account fuel compressor power)	
Net electrical power (kW)	289
Net efficiency	0.64

limit. The operating pressure was assumed in accordance to [18]. In fact, the design point of the HS plant is the operating condition where the microturbine flow rate, rotational speed, pressure, and turbine inlet temperature are all properly matched to guarantee the design performance of the plant, and its safe operation [19]. The ejector has been designed to ensure the proper STCR value avoiding carbon deposition inside the reformer and the cell. Table 1 reports the main design point values.

It is important to underline that the HS efficiency is 64%, which is particularly significant considering the small size (289 kW$_e$) of the whole plant. Such efficiency is even better than that of advanced large combined cycle (>200 MW) plants, using steam as the blade-cooling medium.

The comparison of this design point with other previous design studies [2,19] is a first verification of the TRANSEO model. In fact, the ratio between mGT and HS power, that is 17%, is very close as well as the ratio between mGT and SOFC power that is 21% [19].

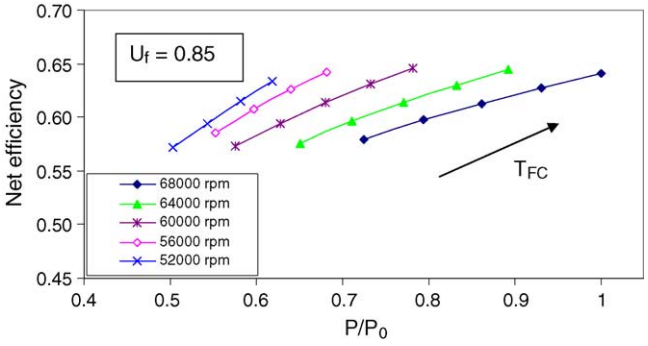

Fig. 10. Plant net efficiency.

4.2. Off-design analysis

The hybrid system transient model was successfully verified at off-design conditions, comparing the results with some previous studies [2,19]. Even if the design point is not exactly the same, the off-design behaviour is similar. In fact, Figs. 10 and 11, which represent steady-state conditions reached with the transient model, show the same trends as the results obtained with an off-design model [2,19]. Each point verifies the operative limitations of the plant [19]. In fact, it is absolutely necessary to avoid cell temperatures that are too high or too low, an operating condition too close to the compressor surge line (surge margin) and mGT overspeed [2].

4.3. Transient behaviour

The behaviour of the entire cycle, resulting from the reduction of the fuel ejector nozzle total pressure by a step of 10%, operating at microturbine constant rotational speed and maintaining the fuel utilization coefficient fixed at 0.85, has been simulated.

The results are not only an example of the code capabilities, but also represent an interesting operating case because the fuel control is mandatory for the regulation of the HS power. The control system is assumed to be able to control the shaft rotational speed, keeping it constant during the whole transient (for instance, using a by-pass valve or regulating the power extracted from the shaft).

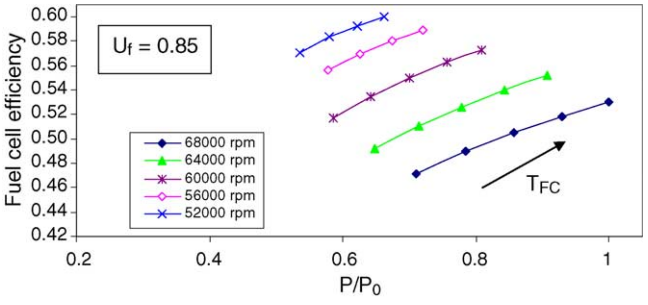

Fig. 11. SOFC efficiency ($\eta_{FC} = P_{FC}/(\dot{m}_{fuel} \times LHV_{fuel})$) in the hybrid system.

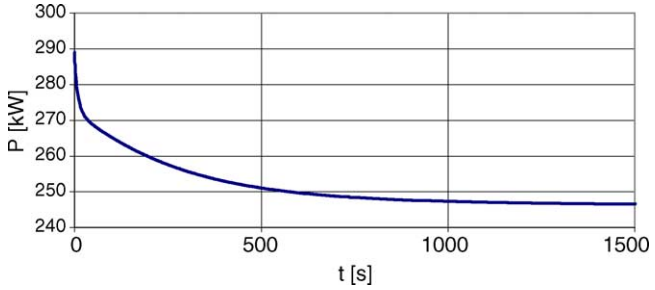

Fig. 12. Hybrid system electrical power (fuel compressor power included).

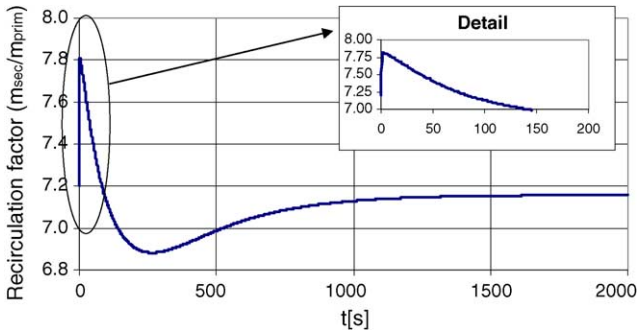

Fig. 13. Ejector recirculation factor.

Of course, the next step would be the testing of different control strategies or control system parameters applied to the present plant model, but this is the topic of further investigations that are now possible with the present HS transient model.

The results show that while the cathodic side is driven only by the temperature variation, because of the rotational speed being assumed constant, the anodic side is characterized by three different time-scale phenomena. In fact, the plant power (Fig. 12) and the ejector recirculation factor (Fig. 13) show the negligible fluid dynamic delay, the depressurisation time delay and the thermal long time-scale effect.

This behaviour is explained by the anodic inlet pressure trend (Fig. 14) and by the SOFC average temperature (Fig. 15). In fact, Fig. 14 shows the depressurisation transient (about 100 s) and the long time-scale temperature variation due to the SOFC thermal inertia, whose characteristic time is about 300 s.

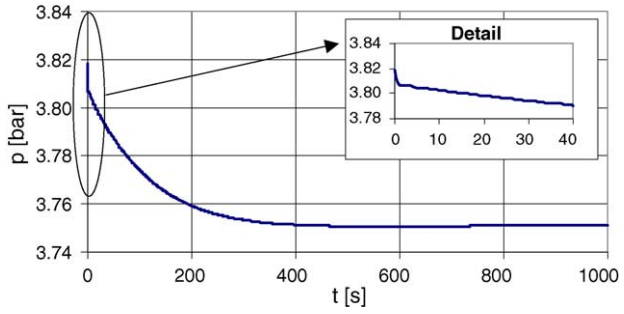

Fig. 14. Anodic inlet pressure.

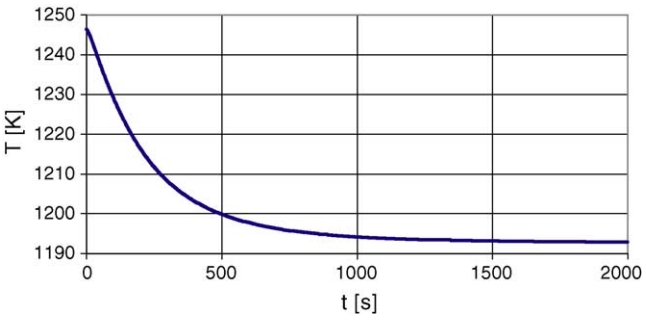

Fig. 15. SOFC average temperature.

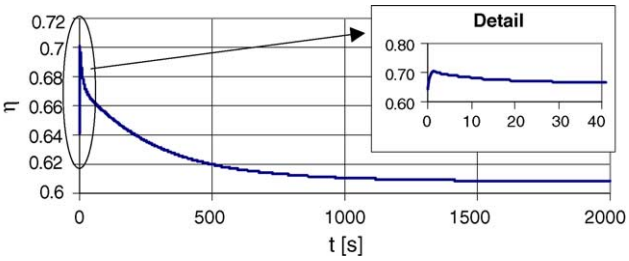

Fig. 16. Plant net efficiency.

The efficiency of the system (Fig. 16) shows a trend that is a direct consequence of the HS power behaviour. In fact, the sudden increase due to the fuel step is followed by a smooth decrease toward the new steady-state condition. The latter transient is mainly driven by the depressurisation and the thermal inertia of the fuel cell.

The main objective of the analysis is the verification of the fuel cell behaviour inside the whole plant, since it is the most expensive component affected by relevant operational constraints. Albeit the differential pressure between the anodic and the cathodic side is never too high (Fig. 17) and the fuel cell inlet STCR (Fig. 18) is always within an acceptable range, Figs. 17 and 18 show that a greater fuel variation could create some problems, especially during transient conditions: in fact, the oscillation of the STCR and the maximum differential pressure could become unacceptable. So, it seems advisable for the control system to act on the microturbine rotational speed to reduce the cathodic pressure, limiting the pressure difference between the anodic and the cathodic side of the cell.

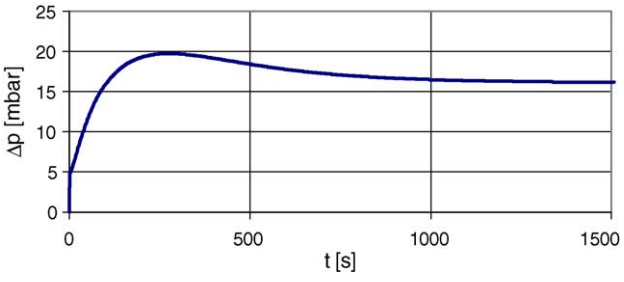

Fig. 17. Differential pressure between the anodic and the cathodic side (at design point such a differential pressure has to be minimized).

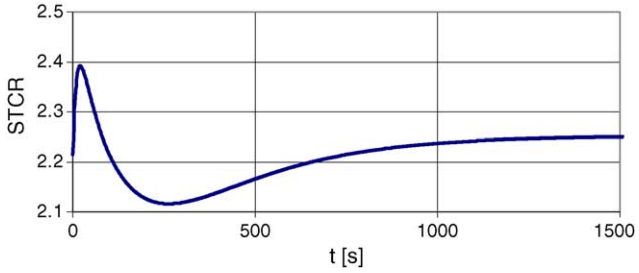

Fig. 18. Fuel cell inlet steam-to-carbon ratio.

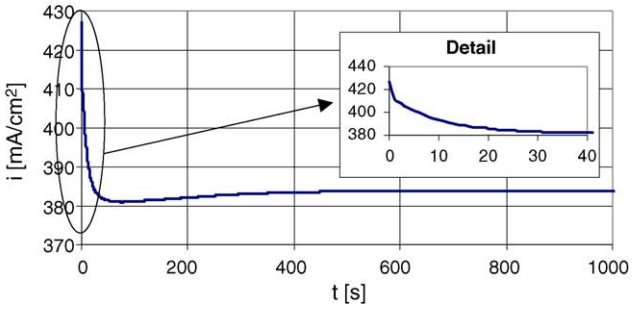

Fig. 19. Fuel cell average current density.

Fig. 19 reports the average current density behaviour: it shows the fast fluid dynamic delay (<1 s), the effect of the depressurisation delay (100 s) and the thermal inertia as well (300 s). Another significant parameter is the stack voltage (Fig. 20), which is reduced because the total electrical resistance is increased by the temperature decrease. Instead, the initial peak is due to the rapid decrease in current density.

On the cathodic side the reduction in the fuel cell average temperature produces an increase in the mass flow rate (Fig. 21) and a decrease in the pressure ratio (Fig. 22). Such a new steady-state condition is well explained by the compressor characteristic curve (Fig. 23).

The compressor operating point moves to lower pressure ratio values, also achieving a larger surge margin (Fig. 24). As expected, the reduction of the fuel flow rate (at turbomachinery constant rotational speed) does not create problems for the compressor because it moves away from the surge line.

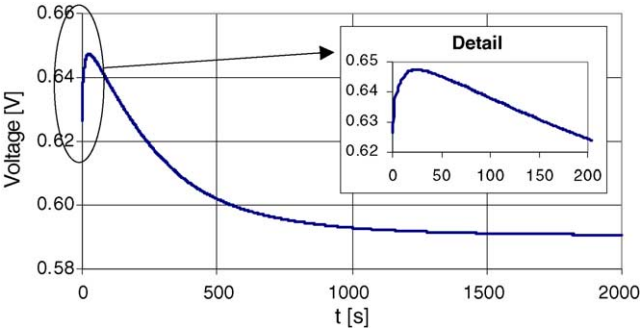

Fig. 20. Fuel cell voltage.

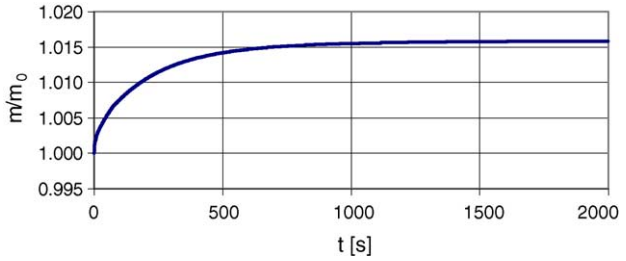

Fig. 21. Air compressor mass flow rate.

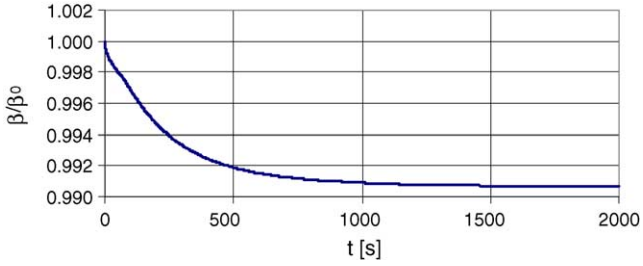

Fig. 22. Air pressure ratio.

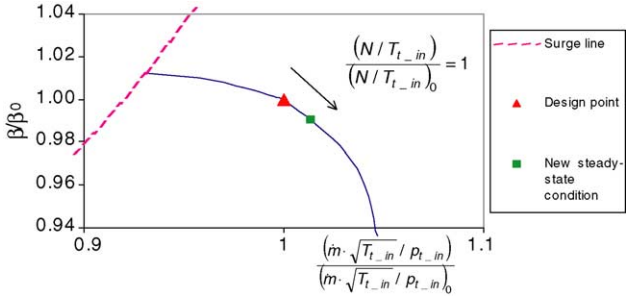

Fig. 23. Compressor characteristic map and operative point.

The temperature variation in the metal matrix of the recuperator needs to be carefully monitored, in order to keep the thermal stress under control. Fig. 25 shows the heat flux behaviour over time. The difference between the curves reported in Fig. 25 is due to the thermal storage within the recuperator matrix. Even if the detailed temperature distribution is known, the effect is also evident in the matrix average temperature variation (Fig. 26), which, however, does not seem

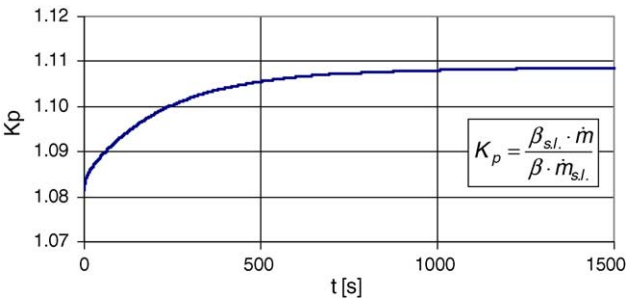

Fig. 24. Surge margin.

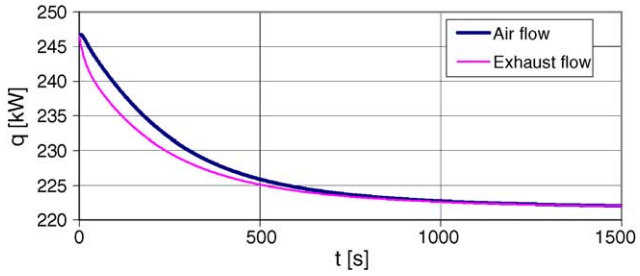

Fig. 25. Recuperator heat fluxes.

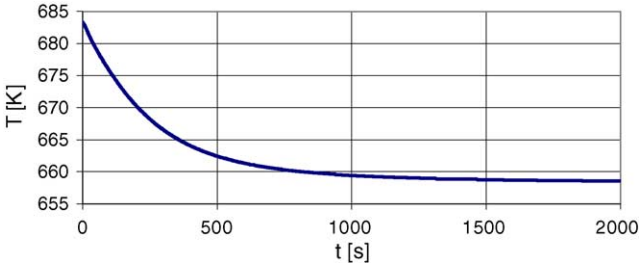

Fig. 26. Recuperator matrix average temperature.

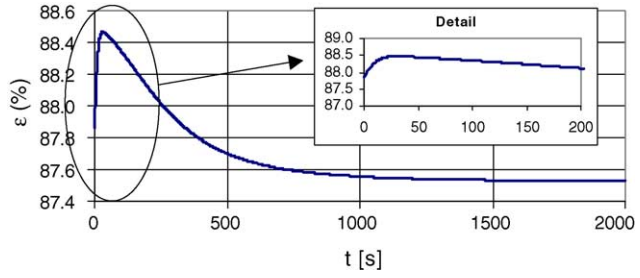

Fig. 27. Recuperator effectiveness.

to be critical in this case (maximum temperature gradient of about 0.1 K s^{-1}).

Another meaningful property is the recuperator effectiveness, reported versus time in Fig. 27. The rapid increase is due to the initial variation in the TOT, which is caused by the depressurisation of the cell. Such an apparent increase in effectiveness is simply due to the recuperator thermal inertia, because the matrix releases part of the heat that is stored internally.

5. Conclusions

This work has been carried out at TPG, University of Genoa, in order to analyse the transient behaviour of a SOFC hybrid system based on the coupling of a recuperated micro-gas turbine with a tubular solid oxide fuel cell, giving special attention to the anodic recirculation performance over time. The main conclusions and results of the study are:

- The "dynamic" and "lumped volume" ejector models for SOFC recirculation circuit have been developed and successfully tested and validated.
- The SOFC hybrid system transient model has been developed with TRANSEO, a tool developed at TPG [14]. It has been successfully verified at design and off-design conditions.
- Special attention has been devoted to properly modelling the composition variation over time for all the components of the plant.
- The time-scales of the main transient phenomena have been calculated: the very short fluid dynamic time- scale (less than 1 s), the pressurization/depressurisation characteristic time (about 100 s) and the fuel cell and heat exchanger thermal inertia long time-scale (over 300 s). They should be taken into account for the development of a proper control system.
- During transients, unexpected fluctuations in important proprieties, such as STCR, could occur and need to be carefully monitored, in order to avoid the system running into "forbidden" or "dangerous" areas.

The transient model presented here is currently being used for IP-SOFC system modelling [19,20] and for hybrid system control definition.

Acknowledgements

This work has been partially founded by MIUR of Italy through the FISR-2000-107/RIC contract, National Coordinator A.F. Massardo, and by MIUR-PRIN-2003 contract, Responsible A. Bosio.

References

[1] P. Costamagna, L. Magistri, A.F. Massardo, Design and part-load performance of a hybrid system based on a solid oxide fuel cell reactor and a micro gas turbine, J. Power Sources 96 (2001) 352–368.
[2] L. Magistri, Hybrid system for distributed generation, Ph.D. thesis, TPG-DiMSET, University of Genoa, 2003.
[3] A. Traverso, F. Calzolari, A.F. Massardo, Transient behavior of and control system for micro gas turbine advanced cycles, ASME Paper 2003-GT-38269, accepted for Transactions.
[4] F. Marsano, L. Magistri, A.F. Massardo, Ejector performance influence on a solid oxide fuel cell anodic recirculation system, J. Power Sources 129 (2003) 216–228.
[5] R.W. MacCormack, The effect of viscosity in hypervelocity impact cratering AIAA paper no.69-354, Cincinnati, Ohio, 1969.
[6] C. Cravero, A.F. Massardo, A Gas turbine compressor simulation model for inclusion of active control strategies, in: RTO Symposium on Active Control Technology for Enhanced Performances Operational Capabilities of Military Aircraft, Land Vehicles and Sea Vehicles, Braunschweig, 8–11 May 2000.
[7] G. Moretti, Importance of boundary condition in the numerical treatment of hyperbolic equations, The physics of fluids, supplement II, NASA Technical Report, 1968.
[8] M.J. Abbet, Boundary Condition Calculation Procedures for Inviscid Supersonic Flow Fields, AIAA Paper, Palm Springs, CA, 1973.

[9] M.L. Ferrari, Dynamic model of the anodic side recirculation of solid oxide fuel cells in hybrid systems, Master thesis degree, TPG-DiMSET, University of Genoa, 2003 (in Italian).
[10] C.A.J. Fletcher, Computational Techniques for Fluid Dynamics, vol. 1, Springer-Verlag, 1991.
[11] E. Cerelli, Experimental analysis of a microturbine pilot plant with thermal energy recovery, Master thesis Degree, TPG-DiMSET, University of Genoa, 2002 (in Italian).
[12] B. Gerald, G. Hill, P. Hill, Analysis and testing of two-dimensional, slot nozzle ejectors with variable area mixing sections, NASA contractor report, 1973, pp. 95–129.
[13] H. McMahon, J. Jagoda, N. Komerath, J. Seitzman, Transient Measurement in a Shock Tube, Georgia Tech College of Engineering, School of Aerospace Engineering, 1999–2000.
[14] A. Traverso, TRANSEO: a new simulation tool for transient analysis of innovative energy systems, Ph.D. thesis, TPG-DiMSET, University of Genoa, March 2004.
[15] R.A. Roberts, F. Jabbari, J. Brouwer, R.S. Gemmen, E.A. Liese, Inter-laboratory dynamic modelling of a carbonate fuel cell for hybrid application, ASME Paper 2003-GT-38774, 2003.
[16] A. Traverso, L. Magistri, R. Scarpellini, A.F. Massardo, Demonstration plant and expected performance of an externally fired micro gas turbine for distributed power generation, ASME Paper 2003-GT-38268, 2003.
[17] S.C. Singhal, Advances in solid oxide fuel cell technology, Solid State Ionics 135 (2000) 305.
[18] J.H. Hirscenhofer, D.B. Stauffer, R.R. Engleman, M.G. Klett, Fuel Cell Handbook, DOE report DOE/FETC-99/1076, US Department of Energy, Morgantown (WV), 1998.
[19] L. Magistri, M. Bozzolo, O. Tarnowski, G. Agnew, A.F. Massardo, Design and off-design analysis of a mw hybrid system based on rolls-royce integrated planar SOFC, ASME Paper 2003-GT-38220, 2003.
[20] PIP-SOFC European Project NNE5-2001-00791, Technical Meeting, Paris, November 2003.